

^{15}N Chemical Shift Tensors of Uracil Determined from ^{15}N Powder Pattern and ^{15}N – ^{13}C Dipolar NMR Spectroscopy

Karen L. Anderson-Altmann,[†] Cu G. Phung, Stylianos Mavromoustakos, Zhiwen Zheng, Julio C. Facelli,[‡] C. Dale Poulter, and David M. Grant*

Department of Chemistry and Utah Supercomputing Institute, University of Utah, Salt Lake City, Utah 84112

Received: July 12, 1994; In Final Form: February 27, 1995[⊗]

The ^{15}N chemical shift tensors of uracil are reported using ^{15}N powder pattern techniques. The principal values of the ^{15}N uracil tensors are obtained from the spectra of $[1-^{15}\text{N}]\text{uracil}$ and $[3-^{15}\text{N}]\text{uracil}$, and the tensor orientations are determined from the spectrum of $[1,3-^{15}\text{N}_2,2-^{13}\text{C}]\text{uracil}$ by including the effects of the direct dipolar interaction in the spectral fitting routine. Ambiguities in the orientational assignments, which arise from the axial symmetry of the direct dipolar tensor, are resolved using molecular symmetry considerations and results of *ab initio* calculations of ^{15}N chemical shielding tensors. The N_1 nitrogen has principal values of 196, 114, and 30 ppm and the N_3 nitrogen 200, 131, and 79 ppm with respect to $^{15}\text{NH}_4\text{NO}_3$. Assuming that the smallest (most shielded) chemical shift tensor components are oriented perpendicular to the molecular plane, the largest components are found to lie 18° and 9° off the $\text{N}_1\text{—H}$ and $\text{N}_3\text{—H}$ bonds, respectively, rotated toward C_2 and C_4 . These orientations are in good agreement with those calculated theoretically. In addition, inclusion of intermolecular hydrogen bond effects in the theoretical calculations significantly improves the correlation between the calculated and experimental principal values.

Introduction

Uracil is one of the four heterocyclic bases found as subunits of the nucleotides in RNA. The hydrogen bonding between uracil and adenine is important in the synthesis of mRNA from DNA and in the translation of the genetic code via tRNA. Guanine–uracil hydrogen-bonded base pairs are involved in the tertiary structure of tRNA and in codon–anticodon interactions. Nuclear magnetic resonance is a very useful tool for the study of hydrogen bonding, since the chemical shift of a magnetically active nucleus is sensitive to the surrounding electronic environment. This is particularly true of the ^{15}N nucleus, due to the lone pair of electrons, which provides a broader range of bonding possibilities and thus a greater sensitivity of chemical shielding to changes in electronic characteristics. Nitrogen nuclei play an active role in the hydrogen bonding of all of the base pairs, so ^{15}N NMR should provide useful information about the extent of hydrogen bonding in these systems.

The effects of A:U base pairing on the ^{15}N chemical shifts of each species have been investigated in solution,^{1–3} where significant changes have been observed upon pair formation, even for the N_3 nucleus of adenine, which is not located at an interaction site. Using the technique of ^1H – ^{15}N multiple-quantum NMR, the A:U and G:U pairs in *Escherichia coli* 5S RNA have been identified by selectively labeling the N_3 position of the uridines.⁴ Information on the anisotropy of the chemical shielding interaction has the potential of providing an even better understanding of the electronic environment around a nucleus and how it is affected by hydrogen-bonding interactions, particularly if the orientation of the principal values of the chemical shift tensor can be determined. One way to obtain such orientational information is through the combined dipolar–chemical shift experiment,^{5,6} which relies on the magnetic coupling of the nucleus of interest to another nucleus possessing

a spin. The resulting dipolar–chemical shift interaction affects the observed powder pattern.

In order to understand the spectra of interacting base pairs, one must first obtain and interpret the spectra of the isolated, nonpairing molecules. In this paper, the ^{15}N chemical shift tensors, including principal values and orientations, of the two nitrogens in uracil are reported. The only other complete determinations of ^{15}N chemical shift tensors of aromatic nitrogens are for L-histidine hydrochloride monohydrate⁷ and the tryptophan residue of fd bacteriophage,⁸ whereas the principal values alone have been determined for pyridine⁹ and histidine.¹⁰ While previously calculated,¹¹ this is the first experimental measurement of the ^{15}N chemical shift anisotropies of ring nitrogens in any of the heterocyclic bases. Thus, this work provides a model for ^{15}N chemical shift tensors in these types of systems.

Experimental and Computational Methods

Materials. Propiolic acid and polyphosphoric acid (PPA) were purchased from Aldrich Chemical Co. Unlabeled urea was purchased from Sigma Chemical Co. $[^{13}\text{C},^{15}\text{N}_2]\text{urea}$ (99%) was purchased from Cambridge Isotope Laboratories. $[1-^{15}\text{N}]\text{uracil}$ and $[3-^{15}\text{N}]\text{uracil}$, prepared using the procedure of Roberts and Poulter,¹² were available from earlier studies in the Poulter laboratory.

Synthesis of $[1,3-^{15}\text{N}_2,2-^{13}\text{C}]\text{Uracil}$. The procedure used was based on that originally described by Harada and Suzuki.¹³ In a 100 mL round-bottomed flask a mixture of 0.50 g of $[^{13}\text{C},^{15}\text{N}_2]\text{urea}$ (7.93 mmol), 0.58 g of propiolic acid (8.28 mmol), and 12 g of polyphosphoric acid was heated at 85°C for 4 h with occasional stirring. The mixture was cooled in an ice–water bath, and water (24 mL) was added gradually as a precipitate formed. The mixture was maintained at approximately 5°C for 24 h. The precipitate was collected by filtration and placed under high vacuum (0.01 mmHg) over P_2O_5 to give 0.73 g (80% yield) of a white solid. ^1H , ^{13}C , and ^{31}P NMR spectra showed the presence of a single product.

[†] Current address: Chemistry and Materials Branch, Code 474230D, Naval Air Warfare Center Weapons Division, China Lake, CA 93555.

[‡] Utah Supercomputing Institute.

[⊗] Abstract published in *Advance ACS Abstracts*, May 15, 1995.

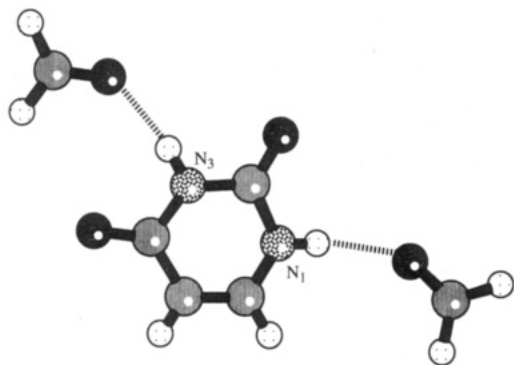


Figure 1. Model of uracil hydrogen-bonded to two H₂CO molecules.

Acquisition of NMR Data. All experiments were performed at room temperature on a modified Varian VXR-200 NMR spectrometer equipped with an Oxford superconducting magnet. A rotor containing approximately 100 mg of sample was placed in a Doty 7 mm magic angle spinning solids probe. Typical spinning speeds of 5 kHz were used to obtain the isotropic data. A spin-echo, cross-polarization, ¹H decoupling pulse sequence was used. An echo delay of 50 μs and a contact time of 3 ms were employed. The decoupling field strength was 45 kHz. All spectra are referenced to ¹⁵NH₄NO₃ at room temperature (20 °C) at a spin rate of 1 kHz. By convention, the highest shift component is designated as δ₁₁ and the lowest shift as δ₃₃, so that in ppm from the reference δ₁₁ > δ₂₂ > δ₃₃.

Calculations. *Ab initio* calculations of the chemical shielding tensors were performed on a cluster of IBM/RS6000 Model 370 workstations using the TEXAS 90 program,¹⁴ which implements the Gauge Invariant Atomic Orbital (GIAO) method.¹⁵ A number of basis sets ranging from double-zeta quality to those including diffuse and polarization functions on all the atoms were used in this study to test the sensitivity of the results to the quality of the basis set. The coefficients and exponents were taken from Dunning's compilation.¹⁶ In view of recent work that demonstrated the importance of the molecular structure in the calculation of chemical shift tensors,¹⁷ four different wave functions were used for the calculations based on the following presumed structures: (I) the crystal X-ray diffraction structure,¹⁸ (II) the minimum-energy structure obtained using the HONDO program¹⁹ with the D95 basis set, (III) the X-ray structure of uracil with two formaldehyde molecules added to simulate the hydrogen bonds between the nitrogen nuclei and the oxygens on neighboring uracil molecules, and (IV) the same structure as III, but with the positions of the hydrogens involved in the hydrogen bond optimized by Hartree-Fock quantum mechanical calculations using the D95 basis set. In structure III, illustrated in Figure 1, and also in structure IV the positions of the oxygen and carbon atoms of the formaldehyde molecules correspond to the positions of carbonyl atoms in the neighboring uracil molecules. These positions were taken from the X-ray structure.

Spectral Simulations

The interactions in the ¹⁵N₁-¹³C₂-¹⁵N₃ spin system can be simplified by the following considerations: (1) the low γ of ¹⁵N and the 2.24 Å separation between N₁ and N₃ allow the ¹⁵N-¹⁵N dipolar interaction to be ignored (e.g., calculations predict a dipolar coupling constant of only about 100 Hz); (2) the large difference in the Larmor frequencies of ¹³C and ¹⁵N (30 MHz) compared to the strength of the remaining ¹³C-¹⁵N dipolar interactions (approximately 1200 Hz) allows the non-secular terms in the spin Hamiltonian matrix to be ignored. With these simplifying assumptions, the resultant Hamiltonian, which corresponds to the superposition of two independent chemical

shift dipolar powder patterns,²⁰ contains only Zeeman and nitrogen-carbon direct dipolar terms and is given by^{5,6}

$$\hat{\mathcal{H}} = -\nu_1 I_{z_1} - \nu_2 I_{z_2} - \nu_3 I_{z_3} + A_{12} I_{z_1} I_{z_2} + A_{23} I_{z_2} I_{z_3} \quad (1)$$

where the spin-labels refer to the respective nuclei in the three-spin system. The ν_{*i*} are defined as⁶

$$\nu_i = \mathbf{r}_i'^T \cdot \hat{\nu}_i \mathbf{r}_i' \quad \text{and} \quad \hat{\nu}_i = \left(\frac{\gamma_i}{2\pi} \right) \vec{\mathbf{B}}_0 \cdot (\hat{\mathbf{1}} + \hat{\delta}_i) \quad (2)$$

where δ_{*i*} is the chemical shift tensor of nucleus *i*, *r*'_{*i*} is the unit vector that projects δ_{*i*} along the direction of the magnetic induction, B₀, which includes both the shift reference and susceptibility corrections. The vector *r*'_{*i*}^T is the transpose of *r*'_{*i*}. The A terms in eq 1 are given by

$$A_{AB} = \mathbf{r}''^T \cdot \mathbf{D}_{AB} \cdot \mathbf{r}'' \quad (3)$$

where **D** is the direct dipolar tensor, *r*'' is the unit vector that projects **D** along the direction of B₀, and *r*''^T is the transpose of *r*''.

Using eq 1 and the spin basis sets for three spins of spin 1/2, the energy levels of the system can be readily determined. The frequencies of the allowed transitions are then calculated for a given orientation of the molecule in B₀. The four transitions in the ¹⁵N spectrum are given as

$$\nu_{N_1}^{\pm} = \nu_1 \pm 1/2 A_{12} \quad (4)$$

and

$$\nu_{N_3}^{\pm} = \nu_3 \pm 1/2 A_{32} \quad (5)$$

where the + or - refer to coupling to an α or β carbon spin, respectively. After transforming all of the interaction tensors into the same reference frame and performing a powder average,⁶ the resultant ¹⁵N spectrum will consist of an overlap of two asymmetric doublets of powder patterns, one for each of the spins N₁ and N₃.

In the selected coordinate system, the z-axis of the direct dipolar tensor is placed along the A-B bond, and **D** has the following form:

$$\mathbf{D}_{AB} = \begin{bmatrix} -1/2 D_{AB} & 0 & 0 \\ 0 & -1/2 D_{AB} & 0 \\ 0 & 0 & D_{AB} \end{bmatrix} \quad (6)$$

where D_{AB}, in frequency units, is given by

$$D_{AB} = \left(\frac{\mu_0}{8\pi^2} \right) \frac{\gamma_A \gamma_B \hbar}{r_{AB}^3} \quad (7)$$

and μ₀ is the permeability of free space.

Results and Discussion

The static powder patterns of [1-¹⁵N]- and [3-¹⁵N]uracil are displayed in Figures 2 and 3, respectively, along with the least-squares fit of the data using the POWDER²¹ software. The results of these fits are summarized in Table 1. The δ_{ave} from the powder patterns agree within their experimental errors (±2 ppm) with the δ_{iso} values obtained from CP/MAS spectra. These values also are compatible with the solution values of 111.2 and 138.8 ppm²² and therefore reflect the same structural features present in the liquid state.

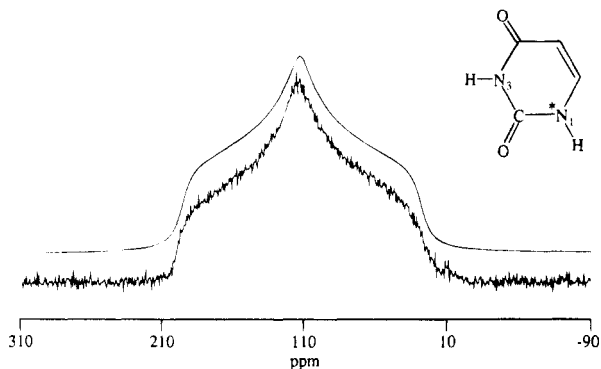


Figure 2. ^{15}N static powder spectrum of $[1-^{15}\text{N}]$ uracil. The lower plot is the experimental spectrum, and the upper plot is the best-fit simulated spectrum. Frequencies are referenced to $^{15}\text{NH}_4\text{NO}_3$.

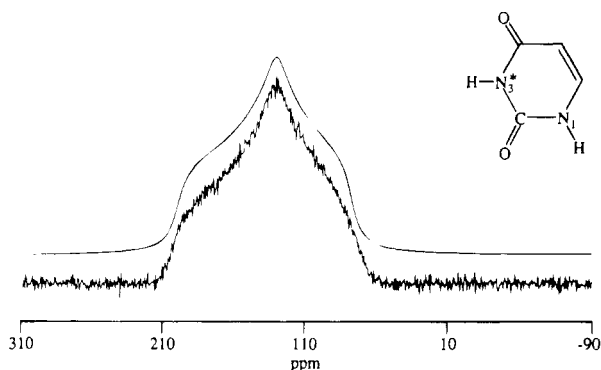


Figure 3. ^{15}N static powder spectrum of $[3-^{15}\text{N}]$ uracil. The lower plot is the experimental spectrum, and the upper plot is the best-fit simulated spectrum. Frequencies are referenced to $^{15}\text{NH}_4\text{NO}_3$.

TABLE 1: Principal Values of the ^{15}N Chemical Shift Tensors in Uracil; All Values Are Given in ppm Relative to Solid $^{15}\text{NH}_4\text{NO}_3$ (Phase IV)

| | ϕ^a | δ_{11} | δ_{22} | δ_{33} | δ_{ave} | δ_{iso}^b | δ_{liq}^c |
|--------------|----------|---------------|---------------|---------------|-----------------------|-------------------------|-------------------------|
| N_1 | 18 | 196 | 114 | 30 | 113 | 113.7 | 111.2 |
| N_3 | 9 | 200 | 131 | 79 | 137 | 135.9 | 138.8 |

^a This angle, ϕ (in degrees), is between the δ_{11} direction and N-H bond axes. The δ_{22} direction is perpendicular to the δ_{11} direction in the plane of the molecule and δ_{33} lies perpendicular to the molecular plane. ^b From CP/MAS spectra. ^c From ref 22.

The various contributions to the spectrum of $[1,3-^{15}\text{N}_2,2-^{13}\text{C}]$ uracil are shown in Figure 4. Figure 4, A and B, display the contributions to the pattern from N_1 and N_3 , respectively, while the experimental spectrum of $[1,3-^{15}\text{N}_2,2-^{13}\text{C}]$ uracil is shown in Figure 4C along with the best fit spectrum that was simulated from the sum of (A) and (B). The analysis of this composite spectrum was assisted by the distinctive principal values obtained from the singly-labeled spectra. The δ_{33} component (i.e., the lowest shift) is identified with the direction perpendicular to the molecular plane, based on both previous theoretical¹¹ and experimental^{7,8} evidence. The axial dipolar tensors lie along their respective N-C bonds. Finally, initial estimates of the dipolar coupling constants may be obtained from the bond lengths in the X-ray crystal structure.¹⁸ The relative orientations of the in-plane components of the chemical shift tensors relative to the dipolar axis, which is collinear with the corresponding N-C bond, are defined by the angle between the direction of δ_{11} and the N-C bond direction. Because the dipolar interaction is axially symmetric, there are two possible in-plane orientations⁶ of δ_{11} that would give the same powder spectrum. Fortunately, both theoretical and experimental precedents dictate that the preferred orientational selection is the one lying nearest to the N-H bond. A two-parameter fit of the two angles between

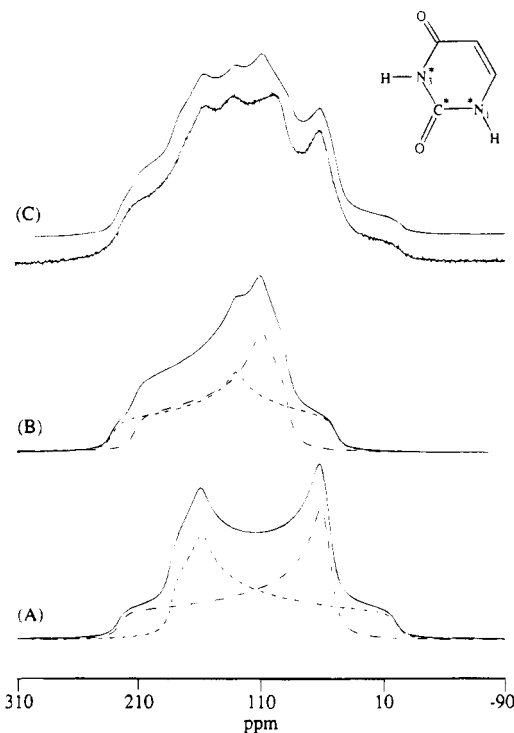


Figure 4. Various contributions to the ^{15}N static powder spectrum of $[1,3-^{15}\text{N}_2,2-^{13}\text{C}]$ uracil. (A) The contributions from the N_1 nitrogens. The two components of the dipolar doublet are given by the dashed lines, and the solid line is the sum of these components. (B) The same as (A) except the contributions are from the N_3 nitrogens. (C) The combined spectrum that results from the sum of (A) plus (B). The lower plot is the experimental spectrum, and the upper plot is the best-fit simulated spectrum. Frequencies are referenced to $^{15}\text{NH}_4\text{NO}_3$.

TABLE 2: Parameters from the Best Fit of the Dipolar Spectrum and Comparison to Known Structural Parameters

| coupled nuclei (A-B) | D_{AB} (measd, Hz) | r_{AB} (calcd, Å) ^a | r_{AB} (lit., Å) ^b |
|-------------------------|--------------------------------|--|---|
| N_1-C_2 | -1265 | 1.343 | 1.371 |
| C_2-N_3 | -1228 | 1.356 | 1.376 |

^a Calculated using eq 7. Note that D_{AB} is negative due to the negative γ of ^{15}N . This change in sign, however, does not affect the appearance of the spectrum. ^b Reference 18.

the dipolar axis and the respective δ_{11} directions for N_1 and N_3 yield computer simulations in good agreement with the experimental spectra. For the final fit, the respective dipolar coupling constants were also allowed to vary, and only minor changes were found in the orientation of the shift tensors.

For reasons of simplicity, the angles, ϕ_i , between δ_{11} and the respective N_i -H bonds are reported in Tables 1 and 3 and in Figure 6. These angles for the two nitrogens are derived from a combination of the X-ray angles between the reported N-H and N-C bonds and from the two fitted angles between δ_{11} and the corresponding N-C dipolar axes. While the errors in the orientation of the dipolar directions relative to the δ_{11} directions are estimated to be less than $\pm 3^\circ$, the uncertainties of the X-ray data for establishing these angles to the N_i -H direction are not included in this estimate. The values of $D_{\text{N}_1-\text{C}_2}$ and $D_{\text{C}_2-\text{N}_3}$ are given in Table 2, along with the calculated internuclear distances, $r_{\text{N}_1-\text{C}_2}$ and $r_{\text{C}_2-\text{N}_3}$. Note that the internuclear distances calculated from the NMR data are slightly smaller than the literature values. This is consistent with the neglect of a small N_1-N_3 dipolar interaction, forcing the fitted $D_{\text{N}_1-\text{C}_2}$ and $D_{\text{C}_2-\text{N}_3}$ values to increase slightly to provide the overall spectral width. In addition, no attempt was made to incorporate any vibrational and/or librational corrections.

TABLE 3: Calculated ¹⁵N Chemical Shielding Principal Values and the In-Plane Orientational Angles of Uracil; Also Given Are Results of the Correlation between the Corresponding Theoretical Shielding Values and the Experimental Principal Shift Values

| structure | N ₁ | | | | N ₃ | | | | slope ^b | intercept ^c | rms ^d | |
|-----------|-----------------|-----------------|-----------------|----------------|-----------------|-----------------|-----------------|----------------|--------------------|------------------------|------------------|--|
| | σ ₁₁ | σ ₂₂ | σ ₃₃ | φ ^a | σ ₁₁ | σ ₂₂ | σ ₃₃ | φ ^a | | | | |
| | D95 | | | | | | | | | | | |
| I | 73.1 | 196.0 | 234.2 | 15.4 | 44.2 | 151.6 | 180.0 | 5.8 | -1.06 | 278.9 | 24.9 | |
| II | 66.0 | 176.6 | 204.7 | 17.0 | 39.7 | 135.9 | 157.8 | 8.7 | -0.92 | 244.9 | 23.9 | |
| III | 65.3 | 180.0 | 237.3 | 15.3 | 37.4 | 136.7 | 187.9 | 7.6 | -1.13 | 282.5 | 17.6 | |
| IV | 58.8 | 160.8 | 220.2 | 17.2 | 33.2 | 121.3 | 173.2 | 9.2 | -1.06 | 260.3 | 14.2 | |
| | D95** | | | | | | | | | | | |
| I | 86.6 | 198.8 | 228.5 | 13.3 | 57.8 | 158.4 | 177.3 | 5.5 | -0.94 | 268.6 | 25.1 | |
| III | 78.5 | 182.7 | 231.6 | 15.5 | 53.0 | 142.7 | 184.8 | 6.9 | -1.01 | 271.4 | 16.9 | |
| | D95++ | | | | | | | | | | | |
| I | 76.1 | 194.0 | 237.6 | 16.2 | 44.0 | 150.0 | 183.8 | 5.8 | -1.07 | 281.7 | 23.1 | |
| III | 69.8 | 178.6 | 238.7 | 15.2 | 37.9 | 138.4 | 189.5 | 8.8 | -1.12 | 282.9 | 17.1 | |
| | D95+++ | | | | | | | | | | | |
| I | 89.0 | 198.3 | 229.5 | 13.8 | 56.9 | 158.6 | 176.6 | 6.1 | -0.94 | 268.6 | 25.3 | |
| III | 82.1 | 183.1 | 232.8 | 14.0 | 51.9 | 145.8 | 184.3 | 8.4 | -1.00 | 272.0 | 17.7 | |
| IV | 75.2 | 165.1 | 207.1 | 16.1 | 47.3 | 130.2 | 165.5 | 12.3 | -0.88 | 242.3 | 16.3 | |

^a Orientational angles, φ (in degrees), between σ₁₁ and the respective N-H bond. In all cases, σ₁₁ is located on the same side of the N-H bond as shown in Figure 6. ^b The negative sign in the slope is due to the inverse dependence of shifts and shieldings. The success of the correlation is measured in part by the agreement between the slope and -1. ^c These intercepts may be compared to the estimated 223.4 ppm absolute chemical shielding of ¹⁵NH₄NO₃, as discussed in the text. ^d rms is the root-mean-square error.

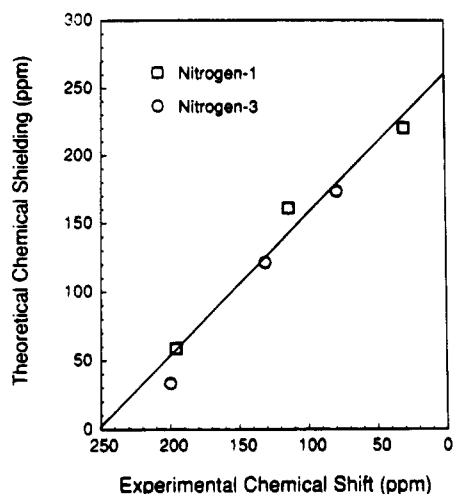


Figure 5. Correlation plot of theoretical chemical shieldings versus experimental chemical shifts. Circles correspond to N₁ data, and triangles correspond to N₃ data. The theoretical values were obtained using structure IV and the D95 basis set. Also shown is the linear least-squares fit of the correlation plot.

The calculated chemical shielding tensors of the nitrogen in uracil are given in Table 3. These results are provided for a variety of structures and basis sets. These theoretical shielding components are plotted against the experimental shifts with the resultant least-squares fitting parameters given in Table 3. A representative plot of one of these many theoretical correlations is given in Figure 5 for the D95 basis set with structure IV. Regardless of the structure or basis set chosen to calculate the various wave functions, the slope remains within about 10% of the ideal correlation value of -1. The negative sign arises because the shift and shielding scales increase in opposite directions. There are no major systematic discrepancies in specific theoretical shielding components, and only modest improvements in these parameters are noted for different structures or basis sets.

The intercepts range from 245 to 283 ppm. This parameter may be compared to the absolute chemical shielding of the reference standard, solid ¹⁵NH₄NO₃ (phase IV), used to define the zero point in ¹⁵N chemical shifts. The absolute chemical shielding of this reference may be estimated from the chemical

shift of nitromethane (358.4 ppm) relative to solid ¹⁵NH₄NO₃ (phase IV). The literature value of the absolute chemical shielding of nitromethane is -135.0 ppm.²³ With the reversal in sign of shieldings and shifts, this approach gives an estimate of +223.4 ppm for the absolute chemical shielding of solid ¹⁵NH₄NO₃ (phase IV). Therefore, the intercepts from the best fits are seen to be somewhat larger than would be expected for the ammonium ion in ¹⁵NH₄NO₃, but the origins of these discrepancies are not presently fully understood. They may reflect systematic errors in the calculations and/or in the procedure used to estimate the absolute chemical shielding of the reference standard.

Examination of the root-mean-square (rms) error between the correlated values and the line of best fit provides insight into the effects of structural and basis set variations. When using the isolated molecule structure (I) to calculate wave functions, the rms errors are approximately 25 ppm regardless of the basis set used in the calculations. Thus, the basis set is not a limiting factor. In comparing the results for structures I and II, it is seen that the rms error is reduced only slightly by the geometric optimization used in II. However, the rms error decreases dramatically for wave functions based on structure III relative to I, indicating that an improvement is made when hydrogen bonding is taken into account with the inclusion of formaldehyde molecules. The smallest rms error is realized for the optimized hydrogen bond positions in structure IV. As observed above in Figure 5, a favorable correlation plot of theoretical versus experimental values was obtained for the D95 basis set and structure IV. With the inclusion of explicit hydrogen-bonded structures, the theory describes adequately the chemical shielding in uracil.

The magnitudes and orientations of the δ_i's obtained from the best fits of the data in Figures 2-4 are displayed in Figure 6. With δ₁₁ lying nearly along the N-H bonds for both N₁ and N₃, one has an experimental measure of the π-bond equivalence on both sides of these two aromatic nitrogens. Also included in Figure 6 are the calculated values (using structure IV at the D95 level) of the angle between δ₁₁ and the two N-H bonds. These theoretical estimates, given in parentheses, are in excellent agreement with the experimental values, supporting the orientational selection used in the fitting program.

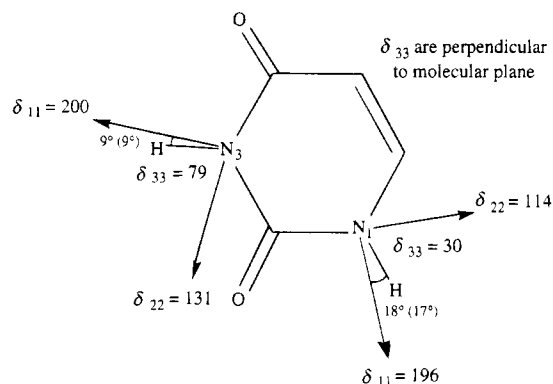


Figure 6. Principal values (in ppm) and orientations of the ^{15}N chemical shift tensors in uracil as determined from the fits in Figures 1–3. Also given, in parentheses, are the theoretically determined orientational angles.

The differences in chemical shift values between the two nitrogens can be understood by considering the electronegativity of the adjoining carbonyl groups. The more electronegative oxygens draw the electron density away from the other atoms in the molecule, causing them to be shifted to higher values. Thus, N_3 , with two neighboring carbonyl groups, has higher shifts than N_1 . This inductive effect is reflected in all three principal values. The orientation of each δ_{11} component along a N–H bond agrees with previous observations that δ_{11} always lies closest to the bond of smallest π -bond order at trigonal sp^2 atoms.²⁴

The principal values and orientations of the ^{15}N chemical shift tensors of uracil compare favorably with those measured in L-histidine hydrochloride monohydrate⁷ and at the protonated nitrogen in histidine.¹⁰ These results add further credence to the well-accepted diketo structure of uracil.²⁵ If other tautomeric forms were contributing to the structure, the corresponding nitrogens would be nonprotonated rather than the protonated type found here, and this would result in a significant increase in the width of the powder pattern (e.g., the nonprotonated nitrogen in cytosine displays an anisotropy of 270 ppm).²⁶

Conclusions

In summary, the ^{15}N chemical shift tensors of uracil are found to have magnitudes and orientations that would be predicted for the diketo structure of uracil, and the principal values are indicative of the protonated type of nitrogen. While the orientations found in uracil are similar to those of aromatic ^{13}C tensors,^{24,27} deviations of the high-shift components are evidence of electronic effects imposed by the presence of the adjoining electronegative carbonyl groups. The theoretically predicted orientations of the principal axes appear to be particularly accurate, an observation that will be useful in studies of related molecules when the orientations cannot be determined experimentally. The agreement of the theoretically determined parameters with the experimental results indicate that the

chemical shift–dipolar data are a sensitive probe of the electronic structure. The theoretical calculations improve dramatically with the inclusion of intermolecular hydrogen bonding in these solid state data. With the general agreement between the average shift values in the solid and the solution states, the solid state evidence also establishes the importance of intermolecular hydrogen bonding for nucleic acid dimers in nonpolar solvents.²⁸

Acknowledgment. The authors gratefully acknowledge the support give by the National Institutes of Health, Grant GM08521, and the National Science Foundation U.S.–Argentina Cooperative Research, Grant INT 86-12463, for this research. Computational resources were partially provided by the Utah Supercomputing Institute.

References and Notes

- (1) Poulter, C. D.; Livingston, C. L. *Tetrahedron Lett.* **1979**, *9*, 755.
- (2) Watanabe, M.; Iwahashi, H.; Sugeta, H.; Kyogoku, Y.; Kuinoshio, M. *Nucleic Acid Res.* **1979**, *6*, 79.
- (3) Watanabe, M.; Sugeta, H.; Iwahashi, H.; Kyogoku, Y.; Kainoshio, M. *Eur. J. Biochem.* **1981**, *117*, 553.
- (4) Davis, D. R.; Yamaizumi, Z.; Nishimura, S.; Poulter, C. D. *Biochemistry* **1989**, *28*, 4105.
- (5) VanderHart, D. L.; Gutowsky, H. S. *J. Chem. Phys.* **1968**, *49*, 261.
- (6) Zilm, K. W.; Grant, D. M. *J. Am. Chem. Soc.* **1981**, *103*, 2913.
- (7) Harbison, G.; Herzfeld, J.; Griffin, R. G. *J. Am. Chem. Soc.* **1981**, *103*, 4752.
- (8) Cross, T. A.; Opella, S. J. *J. Am. Chem. Soc.* **1983**, *105*, 306.
- (9) Schweitzer, D.; Spiess, H. W. *J. Magn. Reson.* **1974**, *15*, 529.
- (10) Munowitz, M.; Bachovchin, W. W.; Herzfeld, J.; Dobson, C. M.; Griffin, R. G. *J. Am. Chem. Soc.* **1982**, *104*, 1192.
- (11) Schindler, M. *J. Am. Chem. Soc.* **1988**, *110*, 6623.
- (12) Roberts, J. L.; Poulter, C. D. *J. Org. Chem.* **1978**, *43*, 1547.
- (13) Harada, K.; Suzuki, S. *Tetrahedron Lett.* **1976**, *27*, 2321.
- (14) Wolinski, K.; Hinton, J. F.; Pulay, P. *J. Am. Chem. Soc.* **1990**, *112*, 1851.
- (15) Ditchfield, R. *Mol. Phys.* **1974**, *27*, 789.
- (16) Dunning, T. H.; Hay, P. J. In *Modern Theoretical Chemistry*; Schaefer, H. F., Ed.; Plenum Press: New York, 1977; Vol. 3, p 1.
- (17) Facelli, J. C.; Grant, D. M. *Nature* **1993**, *365*, 325.
- (18) Stewart, R. F. *Acta Crystallogr.* **1967**, *23*, 1102.
- (19) Dupuis, M. HONDO-8, IBM Corporation, Center for Scientific & Engineering Computations, Department 28B/428, Neighborhood Road, Kingston, NY 12410.
- (20) Wasylishen, R. E.; Curtis, R. D.; Eichele, K.; Lumsden, M. D.; Pender, G. H.; Power, W. P.; Wu, G. In *Nuclear Magnetic Resonance and Molecular Structure*; Tossell, J. A., Ed.; Kluwer: Dordrecht, 1993; p 297.
- (21) Alderman, D. W.; Solum, M. S.; Grant, D. M. *J. Chem. Phys.* **1986**, *84*, 3717.
- (22) Hawkes, G. E.; Randall, E. W.; Hull, W. E. *J. Chem. Soc., Perkin Trans. 2* **1977**, 1268.
- (23) Jameson, C. J.; Mason, J. In *Multinuclear NMR*; Mason, J., Ed.; Plenum Press: New York, 1987; p 56.
- (24) Carter, C. M.; Alderman, D. W.; Facelli, J. C.; Grant, D. M. *J. Am. Chem. Soc.* **1987**, *109*, 2639.
- (25) Kwiatkowski, J. S.; Pullman, B. *Adv. Heterocycl. Chem.* **1975**, *18*, 199.
- (26) Anderson-Altman, K. L. Ph.D. Dissertation, The University of Utah, 1994.
- (27) Orendt, A. M.; Sethi, N. K.; Facelli, J. C.; Horton, W. J.; Pugmire, R. J.; Grant, D. M. *J. Am. Chem. Soc.* **1992**, *114*, 2832.
- (28) Grmeiner, W. H.; Poulter, C. D. *J. Am. Chem. Soc.* **1988**, *110*, 7640.